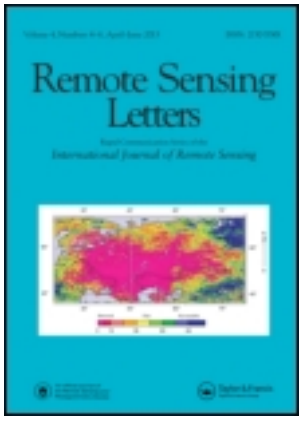

Remote Sensing Letters
Publication details, including instructions for authors and subscription information:
http://www.tandfonline.com/loi/trsl20

A region-growing technique to improve multi-temporal DInSAR interferogram phase unwrapping performance

Y. Yang [a b], A. Pepe [b], M. Manzo [b], F. Casu [b] & R. Lanari [b]
[a] School of Electronic Science and Engineering, National University of Defense Technology, Changsha, 410073, China
[b] Istituto per il Rilevamento Elettromagnetico dell'Ambiente (IREA), Consiglio Nazionale delle Ricerche (CNR), Napoli, 80124, Italy

To cite this article: Y. Yang, A. Pepe, M. Manzo, F. Casu & R. Lanari (2013) A region-growing technique to improve multi-temporal DInSAR interferogram phase unwrapping performance, Remote Sensing Letters, 4:10, 988-997, DOI: 10.1080/2150704X.2013.826835

To link to this article: http://dx.doi.org/10.1080/2150704X.2013.826835

Remote Sensing Letters, 2013
Vol. 4, No. 10, 988–997, http://dx.doi.org/10.1080/2150704X.2013.826835

A region-growing technique to improve multi-temporal DInSAR interferogram phase unwrapping performance

Y. YANG†‡, A. PEPE‡, M. MANZO‡, F. CASU‡ and R. LANARI*‡

†School of Electronic Science and Engineering, National University of Defense Technology, Changsha 410073, China

‡Istituto per il Rilevamento Elettromagnetico dell'Ambiente (IREA), Consiglio Nazionale delle Ricerche (CNR), Napoli 80124, Italy

(*Received 30 April 2013; in final form 11 July 2013*)

We present an efficient solution to mitigate phase unwrapping (PhU) errors that can affect a sequence of multi-temporal differential synthetic aperture radar (SAR) interferograms. To this aim, we propose a strategy that, starting from a properly chosen network of differential interferograms, complements PhU operations with an advanced multi-temporal region-growing (RG) procedure that exploits the space-time relationships among the computed interferograms. In particular, the proposed method implements an iterative procedure that, at each step, allows correcting a sequence of previously unwrapped interferograms at one selected pixel, namely candidate pixel, by exploiting the (unwrapped) phase values at its neighbouring 'seed' pixels (i.e. the ones already correctly unwrapped). Following their estimation, the unwrapped phases are then used to retrieve surface deformation products, such as mean deformation velocity maps and displacement time series, through (advanced) small baseline differential SAR interferometry (DInSAR) techniques. The effectiveness of the presented RG PhU algorithm is demonstrated by analysing a data set of SAR images acquired by the European Remote Sensing (ERS)-1/2 sensors over the megacity area of Istanbul, Turkey.

1. Introduction

Differential synthetic aperture radar interferometry (DInSAR) is a well-established remote-sensing technique that allows the retrieval of spatially dense deformation maps of large areas on Earth by measuring the phase difference (interferogram) of temporarily separated synthetic aperture radar (SAR) images (Gabriel *et al*. 1989). Historically developed to analyse displacements caused by single events (Massonnet and Feigl 1998), DInSAR has gradually been extended to investigate the temporal behaviour of the detected displacements through the generation of deformation time series. In this context, several (advanced) DInSAR approaches have been proposed, which can be mostly grouped in two main categories: (i) the techniques, referred to as persistent scatterer (Ferretti *et al*. 2001, Hooper *et al*. 2004), that work on localized targets by operating on single-look interferograms generated with respect to one reference (master) image and (ii) those that also investigate extended targets, referred to as small baseline (SB) (Berardino *et al*. 2002, Mora *et al*. 2003)

*Corresponding author. Email: lanari.r@irea.cnr.it

approaches, which are based on a combination of multi-temporal DInSAR interferograms computed following a proper selection of SAR data pairs characterized by a small spatial and temporal separation (baseline) between the SAR data acquisition orbits. A well-known approach belonging to the SB class is the one referred to as Small BAseline Subset (SBAS) technique, which allows the generation of mean deformation velocity maps and corresponding displacement time series and may exploit both multi-look (Berardino *et al*. 2002) and single-look (Lanari *et al*. 2004) interferograms.

A common problem to be faced within the DInSAR scenario is represented by the phase unwrapping (PhU) operation that consists in restoring the unknown integral multiple of 2π to be added to the measured phase, which is wrapped onto the range $-\pi$ to π, to get the absolute phase signal. Over the years, much work has been done on two-dimensional (space) PhU, which has resulted in many algorithms that may be generally arranged in three main categories: minimum-norm (Fornaro *et al*. 1997, Ghiglia and Pritt 1998), branch-cut (Goldstein *et al*. 1988) and minimum cost flow (MCF) network (Flynn 1997, Costantini 1998) methods. More recently, the need of analysing long sequences of multi-temporal interferograms for (advanced) DInSAR applications has also promoted the development of new PhU approaches, based on the joint exploitation of the spatial and temporal relationships among the produced DInSAR interferograms (Pepe and Lanari 2006, Hooper and Zebker 2007, Shanker and Zebker 2010, Costantini *et al*. 2012). Among them, a technique that is very well integrated within the SBAS procedure is the one proposed by Pepe and Lanari (2006), which is referred to as extended MCF (EMCF) and represents the space–time extension of the basic MCF approach (Costantini 1998).

In this work, we present a simple and effective PhU procedure for multi-temporal interferograms, implementing a region-growing (RG) strategy. RG is a pixel-based image segmentation method that, starting from a selection of initial seed points that identify a region within the image, allows the region growth by determining whether the set of neighbouring pixels can be added to the region. The proposed RG PhU method complements unwrapping operations carried out on a sequence of multi-temporal differential SAR interferograms (and with no specific requirement on the exploited unwrapping algorithm) and guarantees a drastic improvement of the unwrapping performance, especially in areas with low signal-to-noise ratios, thus leading to a substantial increase in the number of coherent pixels that are detectable through advanced DInSAR analyses. This result is achieved via an iterative procedure that, at each step, allows retrieving the sequence of the unwrapped phase values relevant to one selected pixel of the azimuth/range spatial domain, namely candidate pixel, by exploiting the (unwrapped) phase values at its neighbouring 'seed' pixels (i.e. the ones already correctly unwrapped) and by integrating (for each interferogram) the unwrapped phase differences along the relevant seed/candidate spatial arcs. In particular, the seed/candidate unwrapped phase differences are computed by applying the same temporal PhU strategy exploited by the EMCF algorithm (Pepe and Lanari 2006), which only requires that the selected SAR data pairs form a Delaunay triangulation in the temporal/perpendicular baseline plane.

To illustrate the capability of the proposed multi-temporal RG PhU approach, we present the results achieved on SAR data acquired over the megacity area of Istanbul, Turkey, by the European Remote Sensing (ERS)-1/2 sensors during the 1992–2006 time period.

2. Multi-temporal RG PhU technique

In this section, we present the rationale of the proposed RG PhU technique. We start by introducing the selection process of the interferograms needed for the implementation of the developed procedure. Accordingly, we consider a set of $N+1$ SAR images collected at ordered epochs $(t_0, t_1, \ldots, t_N)$, properly co-registered to a reference image, say the one acquired at t_m, with respect to which we also estimate the temporal $\boldsymbol{T} \equiv [t_0 - t_m, \ldots, t_N - t_m]^{\mathrm{T}}$ and spatial $B_\perp \equiv [b_{\perp 0}, b_{\perp 1}, \ldots, b_{\perp N}]^{\mathrm{T}}$ baseline vectors; note that the latter is relevant to the perpendicular component with respect to the radar line of sight (LOS). Each SAR image can be, then, easily represented by a point in the temporal/perpendicular $\boldsymbol{T} \times \boldsymbol{B}_\perp$ baseline plane, see figure 1(*a*), where we compute a Delaunay triangulation (see figure 1(*b*)); each arc of this triangulation, connecting two different points, identifies an interferometric data pair. Moreover, in order to limit the decorrelation noise artefacts affecting DInSAR interferograms (Zebker and Villasenor 1992), we impose thresholds on the maximum allowed temporal and perpendicular baselines of the SAR data pairs; therefore, we remove from the computed triangulation all the triangles involving at least one 'large' baseline arc. Following the identification of such a sub-triangulation, the relevant set of M SB DInSAR interferograms, namely $\boldsymbol{\Phi} = [\Phi_1, \Phi_2, \ldots, \Phi_M]^{\mathrm{T}}$, is generated. This interferogram sequence is, then, unwrapped by using one of the currently available PhU techniques, thus obtaining the corresponding sequence of unwrapped interferograms, namely $\boldsymbol{\Psi} = [\Psi_1, \Psi_2, \ldots, \Psi_M]^{\mathrm{T}}$.

The developed RG PhU method allows us to 'correct' the PhU errors corrupting the $\boldsymbol{\Psi}$ sequence in correspondence to poorly unwrapped pixels (i.e. candidate), starting from the computed high-quality phases relevant to the pixels for which the

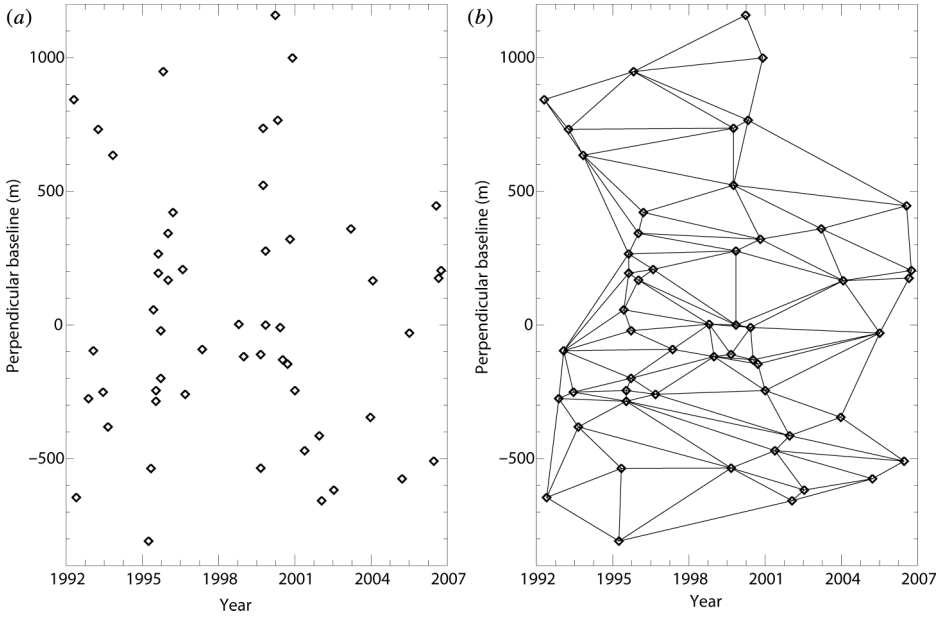

Figure 1. SAR data representation in the temporal/perpendicular baseline plane. (*a*) SAR image distribution. (*b*) Delaunay triangulation after removal of triangles with sides characterized by spatial and/or temporal baseline values exceeding the selected thresholds.

previous unwrapping operation has successfully been accomplished (i.e. seed pixels). Accordingly, the starting point of the proposed RG approach consists in the selection of the seed and candidate pixels. To this aim, we have to introduce a quality index of the PhU retrieval, which is achieved via the following strategy: for each pixel P of the azimuth/range $\left(A_z \times R_g\right)$ spatial plane, we first compute the corresponding deformation time series (without performing any atmospheric filtering operation) by inverting the $\boldsymbol{\Psi}$ unwrapped sequence through the SBAS algorithm (or one of the available advanced SB DInSAR multi-temporal approaches), and then, we estimate the values of the temporal coherence factor (Pepe and Lanari 2006) that is computed as follows:

$$\gamma(P) = \frac{\left|\sum_{i=1}^{M} \exp\left[j\left(\Phi_i(P) - \hat{\Phi}_i(P)\right)\right]\right|}{M} \quad \forall P \in A_z \times R_g \tag{1}$$

where $\mathrm{j} = \sqrt{-1}$ and $\hat{\boldsymbol{\Phi}} = \left[\hat{\Phi}_1, \hat{\Phi}_2, \ldots, \hat{\Phi}_M\right]^{\mathrm{T}}$ is the vector of the (wrapped) interferograms that are reconstructed from the computed deformation time series. At this stage, two sets of pixels are identified: the former, say S, is composed of the N_{S} points (seed pixels) that have temporal coherence values greater than a proper threshold $\hat{\gamma}$: $S \equiv \left\{S^{(i)} \in A_z \times R_g : \gamma\left[S^{(i)}\right] \geq \hat{\gamma}\right\}_{i=1}^{N_{\mathrm{S}}}$; the latter, say C, is made of the N_{C} points (candidate pixels) with coherence values lower than $\hat{\gamma}$: $\mathrm{C} \equiv \left\{C^{(p)} \in A_z \times R_g : \gamma\left[C^{(p)}\right] < \hat{\gamma}\right\}_{p=1}^{N_C}$. Starting from the identified sets of seed and candidate pixels, the proposed RG PhU algorithm implements an iterative procedure that, at the pth iteration, attempts to correct the sequence of the unwrapped phases corresponding to one single candidate pixel, namely $C^{(p)} \in \mathrm{C}$. This result is obtained by taking profit from the knowledge of the K_p correctly unwrapped phase values $\boldsymbol{\Psi}\left(S^{(p,k)}\right)$ corresponding to the seed pixels $S^{(p,k)}, k = 1, \ldots, K_p$ that fall inside a box centred around $C^{(p)}$ (see the inset of figure 2). Accordingly, we have K_p independent phase predictions at $C^{(p)}$, namely $\widehat{\boldsymbol{\Psi}}^{(k)}\left(C^{(p)}\right), k = 1, \cdots, K_p$, obtained by integrating the unwrapped phase difference vectors $\Delta\widehat{\boldsymbol{\Psi}}^{(p,k)} = \Delta\widehat{\boldsymbol{\Psi}}\left(C^{(p)}, S^{(p,k)}\right) \equiv \boldsymbol{\Psi}\left(C^{(p)}\right) - \boldsymbol{\Psi}\left(S^{(p,k)}\right), k = 1, \ldots, K_p$ along the arcs connecting the candidate $C^{(p)}$ and the seed $S^{(p,k)}$ pixels, as pictorially illustrated in the inset of figure 2:

$$\widehat{\boldsymbol{\Psi}}^{(k)}\left(C^{(p)}\right) = \boldsymbol{\Psi}^{(k)}\left(S^{(p,k)}\right) + \Delta\widehat{\boldsymbol{\Psi}}^{(p,k)} \; \forall k = 1, \ldots, K_p \tag{2}$$

To estimate the (unknown) $\Delta\widehat{\boldsymbol{\Psi}}^{(p,k)}$ vectors, we apply the same temporal PhU strategy exploited by the EMCF algorithm (Pepe and Lanari 2006), which is briefly summarized in the following for the sake of completeness. In this case, we introduce a phase model $\boldsymbol{m}^{(p,k)}$ for the $\Delta\widehat{\boldsymbol{\Psi}}^{(p,k)}$ vector, which depends on the temporal $\Delta\boldsymbol{T}$ and perpendicular $\Delta\boldsymbol{B}_{\perp}$ baseline vectors of the exploited sequence of interferometric SAR data pairs:

$$\boldsymbol{m}^{(p,k)}\left(\Delta z^{(p,k)}, \Delta v^{(p,k)}\right) = \frac{4\pi}{\lambda}\frac{\Delta\boldsymbol{B}_{\perp}}{R\sin\vartheta}\Delta z^{(p,k)} + \frac{4\pi}{\lambda}\Delta\boldsymbol{T}\Delta v^{(p,k)} \tag{3}$$

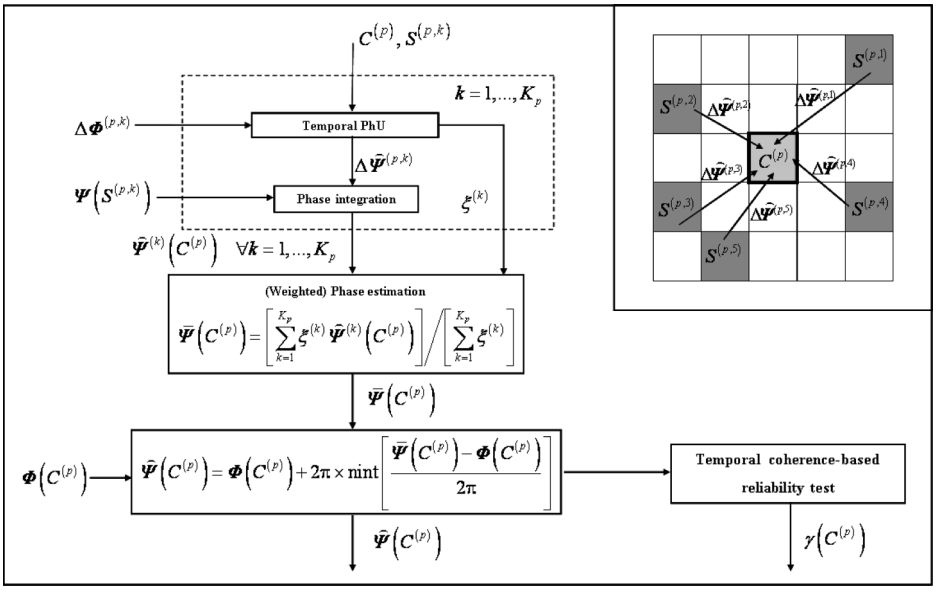

Figure 2. Block-diagram of the iterative RG PhU algorithm. The inset (top right) is a pictorial representation of the pth iteration of the algorithm: the phase values at the candidate pixel $C^{(p)}$ (located at the centre of the grid, light grey box) are predicted by the phases of the five seed pixels $S^{(p,k)}$ (dark grey boxes) located in its neighbourhoods.

where λ is the transmitted signal central wavelength, R is the sensor-to-target distance and ϑ is the incidence angle. Note that the first term on the right-hand side of equation (3) accounts for possible topographic errors $\Delta z^{(p,k)}$, whereas the second one is related to the deformation velocity difference $\Delta v^{(p,k)}$ along the given arc.

Since the $S^{(p,k)}/C^{(p)}$ (unwrapped) phase difference vector $\Delta\widehat{\boldsymbol{\Psi}}^{(p,k)}$ differs from the corresponding wrapped one $\Delta\boldsymbol{\Phi}^{(p,k)} = W\left[\boldsymbol{\Phi}\left(C^{(p)}\right) - \boldsymbol{\Phi}\left(S^{(p,k)}\right)\right]$ by 2π integer multiples (where $W(\cdot)$ represents the modulo-2π wrapping operation), $\Delta\widehat{\boldsymbol{\Psi}}^{(p,k)}$ can be equivalently expressed as $\Delta\widehat{\boldsymbol{\Psi}}^{(p,k)} = \Delta\boldsymbol{\chi}^{(p,k)} + 2\pi\boldsymbol{H}^{(p,k)}$, being $\Delta\boldsymbol{\chi}^{(p,k)} = \boldsymbol{m}^{(p,k)} + W\left(\Delta\boldsymbol{\Phi}^{(p,k)} - \boldsymbol{m}^{(p,k)}\right)$ and $\boldsymbol{H}^{(p,k)}$ an unknown vector of integer multiples. Therefore, for each $\left(\Delta z^{(p,k)}, \Delta v^{(p,k)}\right)$ pair, the $\boldsymbol{H}^{(p,k)}$ unknown vector is evaluated by searching for the solution of the following MCF problem in the $\boldsymbol{T} \times \boldsymbol{B}_{\perp}$ plane (Pepe and Lanari 2006):

$$\begin{aligned} \boldsymbol{H}^{(p,k)} &= \arg\min[\sigma] \\ \sigma &= \frac{1}{M}\sum_{l=1}^{M}\left|\boldsymbol{H}_l^{(p,k)}\right| \end{aligned} \tag{4}$$

subject to the constraints $\boldsymbol{H}_{\alpha}^{(p,k)} + \boldsymbol{H}_{\beta}^{(p,k)} + \boldsymbol{H}_{\gamma}^{(p,k)} = -\text{nint}[(\Delta\chi_{\alpha}^{(p,k)} + \Delta\chi_{\beta}^{(p,k)} + \Delta\chi_{\gamma}^{(p,k)})/2\pi]$, where σ is the network cost; $\boldsymbol{H}_l^{(p,k)}$, $l = \alpha, \beta, \gamma$, are the three elements of the $\boldsymbol{H}^{(p,k)}$ vector, wherein the indexes α, β, γ identify a generic triangle of the

Delaunay triangulation, and nint $(\cdot)$ is the operation of approximation to the nearest integer number.

At this stage, by exploring different values of the $\left(\Delta z^{(p,k)}, \Delta v^{(p,k)}\right)$ pair, we finally evaluate the 'optimal' solution $\Delta\widehat{\boldsymbol{\Psi}}^{(p,k)} = \Delta\boldsymbol{\chi}_{\text{opt}}^{(p,k)} + 2\pi\boldsymbol{H}_{\text{opt}}^{(p,k)}$, where $\Delta\boldsymbol{\chi}_{\text{opt}}^{(p,k)}$ and $\boldsymbol{H}_{\text{opt}}^{(p,k)}$ are the corresponding vectors evaluated in the 'overall' minimum-cost condition, characterized by the minimum cost value $\sigma^{(p,k)} = \min_{\Delta z^{(p,k)}, \Delta v^{(p,k)}}(\sigma) = 1/M \sum_{l=1}^{M} \left| \widehat{\boldsymbol{H}}_{\text{opt},l}^{(p,k)} \right|$.

Following their estimation, we integrate the $\Delta\widehat{\boldsymbol{\Psi}}^{(p,k)}$ vectors over the relevant $S^{(p,k)}/C^{(p)}$ arcs obtaining, for the $C^{(p)}$ candidate pixel, K_p independent phase vector estimates $\widehat{\boldsymbol{\Psi}}^{(k)}\left(C^{(p)}\right)$ (see equation (2)). Then, we carry out a composite prediction of the phase vector at $C^{(p)}$, namely $\overline{\boldsymbol{\Psi}}\left(C^{(p)}\right)$, as the (weighted) average of the computed K_p phase estimates $\widehat{\boldsymbol{\Psi}}^{(k)}\left(C^{(p)}\right)$:

$$\overline{\boldsymbol{\Psi}}(C^{(p)}) = \left[\sum_{k=1}^{K_p} \xi^{(k)} \widehat{\boldsymbol{\Psi}}^{(k)}(C^{(p)})\right] \Bigg/ \left[\sum_{k=1}^{K_p} \xi^{(k)}\right] \tag{5}$$

where the weights $\xi^{(k)}$ are set equal to 1 when $\sigma^{(p,k)} \leq \rho$ and 0 otherwise, being ρ a proper threshold, typically set not greater than 5% of the total number of interferograms (Pepe and Lanari 2006). The retrieved $\overline{\boldsymbol{\Psi}}(C^{(p)})$ is eventually used to obtain the unwrapped phase values at $C^{(p)}$, which are computed following the lines of Xu and Cumming (1999) as

$$\widehat{\boldsymbol{\Psi}}\left(C^{(p)}\right) = \boldsymbol{\Phi}\left(C^{(p)}\right) + 2\pi \times \text{nint}\left[\frac{\overline{\boldsymbol{\Psi}}\left(C^{(p)}\right) - \boldsymbol{\Phi}\left(C^{(P)}\right)}{2\pi}\right] \tag{6}$$

Finally, a check, aimed at establishing whether the estimated $\widehat{\boldsymbol{\Psi}}\left(C^{(p)}\right)$ in equation (6) is correct, is performed by computing, through equation (1), the temporal coherence value corresponding to the retrieved $\widehat{\boldsymbol{\Psi}}\left(C^{(p)}\right)$ vector; the test is passed when the coherence $\gamma\left(C^{(p)}\right)$ is greater than the given threshold $\hat{\gamma}$. In this case, the pixel $C^{(p)}$ is added to the group of the seed pixels and the so-computed unwrapped phases $\widehat{\boldsymbol{\Psi}}\left(C^{(p)}\right)$ replace the preliminarily unwrapped ones, i.e. $\boldsymbol{\Psi}\left(C^{(p)}\right) = \widehat{\boldsymbol{\Psi}}\left(C^{(p)}\right)$; otherwise, the pixel $C^{(p)}$ is discarded from the following analyses.

The block-diagram of the pth iteration of the proposed RG PhU procedure is shown in figure 2.

3. Experimental results

We have investigated the effectiveness of the proposed RG multi-temporal PhU approach by using a SAR data set composed by 53 images acquired over descending orbits (Track 336, Frame 2781) by the ERS-1/2 satellites from 1992 to 2006, which are pictorially represented in the $\boldsymbol{T} \times \boldsymbol{B}_{\perp}$ plane as shown in figure 1(a). The test-site area includes Istanbul, one of the largest megacities in the world (with more than 10 million inhabitants), located along the strike–slip North Anatolian Fault, which was struck by

the major M_w 7.4 Izmit earthquake on 17 August 1999 (Reilinger *et al*. 2000), causing over the whole region more than 17,000 deaths in addition to severe damage and economic loss. The presented analysis exploits a sequence of multi-temporal DInSAR interferograms, selected as described in the previous section by limiting the maximum perpendicular and temporal baselines of the SAR data pairs to 400 m and 2500 days, respectively. As a result, we retrieved a set of 138 differential SAR interferograms, see figure 1(*b*), computed following a complex multi-look operation with 4 looks in the range direction and 20 looks in the azimuth one (Lanari *et al*. 2007), resulting in a pixel dimension of about 100 m × 100 m.

To investigate the performance of the proposed multi-temporal PhU approach, we previously unwrapped the computed sequence of DInSAR interferograms via the EMCF PhU algorithm and, subsequently, we applied to the unwrapped interferograms the proposed space/time RG procedure. Afterwards, we exploited the SBAS-DInSAR procedure to compute mean deformation velocity maps and displacement time series from both the sequences of unwrapped interferograms (i.e. the EMCF and the EMCF + RG ones). Figures 3(*a*) and (*b*) show the two detected mean deformation velocity maps (in colour), superimposed on a multi-look SAR amplitude image (grey scale) of the area, corresponding to the sequences of EMCF and EMCF + RG unwrapped interferograms, respectively. Note that within the two maps only points with temporal coherence values greater than the selected threshold $\hat{\gamma} = 0.7$, representing a typical value used in SBAS-DInSAR analyses (see, for instance, Manzo *et al*. 2012), are included. As a result, we achieve an increase in the number of coherent pixels of about 300%, passing from ∼15,000 to ∼50,000 coherent pixels. To further emphasize the achieved gain in terms of spatial density of high-quality data, we also computed, see figure 3(*c*), the histograms of the temporal coherence values relevant to the two experiments; the improvement, obtained by applying the RG PhU technique, is evident.

It is worth remarking that figures 3(*a*) and (*b*) show the absolute deformation field, despite what DInSAR usually provides, i.e. measurements referred to one single SAR reference pixel typically located in a non-deforming area. To obtain this result, we exploited the measurements at the global positioning system (GPS) station labelled as KANT (Reilinger *et al*. 2000), whose position is highlighted by a black star in figure 3(*b*). In particular, we corrected the computed SBAS-DInSAR deformation time series relevant to the whole region for the large displacement associated to the Izmit earthquake by using the information provided by this GPS station, properly projected along the radar LOS.

The corresponding mean deformation velocity maps of figures 3(*a*) and (*b*) show, in addition to the co-seismic displacement caused by the Izmit earthquake and associated events, several subsiding areas (often in excess of 10 cm per decade) clearly visible within the western districts of the Istanbul megacity (hosting important infrastructures, such as the international airport) which were also heavily damaged by the earthquake due to localized seismic amplification effects (Akarvardar *et al*. 2009). Of course, these deformation patterns are very easily recognizable in the map of figure 3(*b*), thanks to the increased spatial density of coherent pixels retrieved following the application of the RG PhU procedure. The deformation time series in correspondence to the points labelled as D, E and F in figure 3(*b*) are depicted in figures 3(*d*), (*e*) and (*f*), respectively. In particular, figure 3(*d*) shows the comparison between the SBAS-DInSAR deformation time series retrieved following the

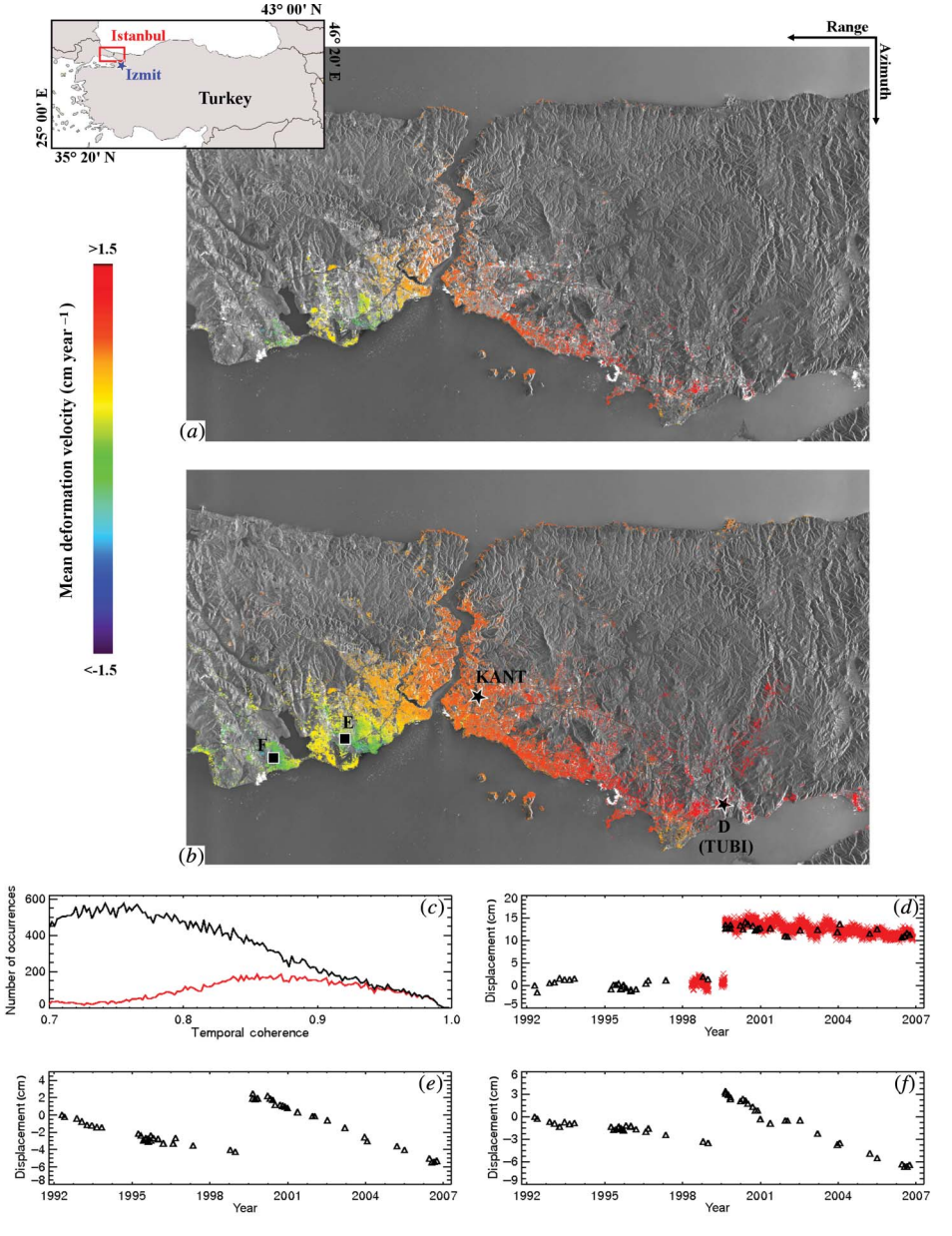

Figure 3. Mean deformation velocity maps (in colour) of the Istanbul megacity area, computed in coherent pixels, only, and superimposed on the SAR amplitude image (grey scale representation) of the zone, retrieved starting from (*a*) the EMCF unwrapped interferograms and (*b*) the EMCF + RG unwrapped ones, respectively. (*c*) Histograms of the temporal coherence maps corresponding to the results reported in figure 3(*a*) (red line) and in figure 3(*b*) (black line). (*d*) Comparison between the retrieved SBAS-DInSAR deformation time series (black triangles) and the LOS-projected GPS time series (red stars) at the location of the TUBI station. (*e*), (*f*) SBAS-DInSAR deformation time series relevant to the two pixels labelled as E and F in figure 3(*b*). Note also that the inset (top left) shows the location of the study area (red rectangle) in Turkey as well as the location (blue star) of the 1999 Izmit earthquake.

application of the EMCF + RG PhU procedures and the one obtained from the LOS-projected measurements at the GPS station labelled as TUBI (http://sopac.ucsd.edu/cgi-bin/refinedTimeSeries-Listing.cgi), located in correspondence to the pixel labelled as D in figure 3*(b)*; the good agreement between the two data is evident, as also testified by the computed standard deviation value $\sigma \approx 1$ cm of the difference between SAR and geodetic measurements. Finally, figures 3(*e*) and (*f*) portray the deformation time series relevant to the two pixels labelled as E and F, located in the western sector of the Istanbul megacity area, and reveal both the effect of the Izmit earthquake and surface subsidence.

4. Conclusions

We have proposed in this work an effective approach to mitigate PhU errors in a properly selected sequence of previously unwrapped multi-temporal DInSAR interferograms by implementing a space–time RG unwrapping procedure, based on the application of the same temporal PhU strategy exploited by the EMCF algorithm. The presented method, which allows expanding well-unwrapped areas to their neighbouring regions characterized by lower signal-to-noise ratios, is straightforwardly applied to sequences of multi-temporal DInSAR interferograms, with no specific requirement on the unwrapping algorithm used to perform the previously unwrapping step, but only on the selection of the interferometric SAR data pairs that have to form a triangulation in the temporal/perpendicular baseline plane. The proposed approach allows retrieving quality-improved sequences of multi-temporal unwrapped interferograms that can be profitably exploited for the generation of surface deformation time series through advanced SB DInSAR approaches. The effectiveness of the presented RG PhU algorithm has been demonstrated by applying the SBAS procedure to a sequence of ERS-1/2 unwrapped interferograms relevant to the Istanbul megacity area.

Acknowledgements

We thank the University of Delft, The Netherlands, and the NASA SRTM mission for providing the satellite orbit state vectors and the digital elevation model of the Istanbul region, respectively. We also thank T.R. Walter for making available the SAR data. This work was carried out under the sponsorship from the programme of China Scholarship Council CSC n. 2010611063.

References

Akarvardar, S., Feigl, K.L. and Ergintav, S., 2009, Ground deformation in an area later damaged by an earthquake: monitoring the Avcilar district of Istanbul, Turkey, by satellite radar interferometry 1992–1999. *Geophysical Journal International*, **178**, pp. 976–988.

Berardino, P., Fornaro, G., Lanari, R. and Sansosti, E., 2002, A new algorithm for surface deformation monitoring based on small baseline differential SAR interferograms. *IEEE Transactions on Geoscience and Remote Sensing*, **40**, pp. 375–2383.

Costantini, M., 1998, A novel phase unwrapping method based on network programming. *IEEE Transactions on Geoscience and Remote Sensing*, **36**, pp. 813–821.

Costantini, M., Malvarosa, F. and Minati, F., 2012, A general formulation for redundant integration of finite differences and phase unwrapping on a sparse multi-dimensional domain. *IEEE Transactions on Geoscience and Remote Sensing*, **50**, pp. 758–768.

Ferretti, A., Prati, C. and Rocca, F., 2001, Permanent scatterers in SAR interferometry. *IEEE Transactions on Geoscience and Remote Sensing*, **39**, pp. 8–20.

Flynn, T.J., 1997, Two-dimensional phase unwrapping with minimum weighted discontinuity. *Journal of the Optical Society of America A*, **14**, pp. 2692–2701.

Fornaro, G., Franceschetti, G., Lanari, R., Rossi, D. and Tesauro, M., 1997, Interferometric SAR phase unwrapping using the finite element method. *IEE Proceedings of Radar, Sonar and Navigation*, **144**, pp. 266–274.

Gabriel, A.K., Goldstein, R.M. and Zebker, H.A., 1989, Mapping small elevation changes over large areas: differential interferometry. *Journal of Geophysical Research*, **94**, pp. 9183–9191.

Ghiglia, D.C. and Pritt, M.D., 1998, *Two-Dimensional Phase Unwrapping: Theory, Algorithms, and Software* (New York: Wiley).

Goldstein, R.M., Zebker, H.A. and Werner, C.L., 1988, Satellite radar interferometry: two-dimensional phase unwrapping. *Radio Science*, **23**, pp.713–720.

Hooper, A. and Zebker, H., 2007, Phase unwrapping in three dimensions, with application to InSAR time series. *Journal of the Optical Society of America A*, **24**, pp. 2737–2747.

Hooper, A., Zebker, H., Segall, P. and Kampes, B., 2004, A new method for measuring deformation on volcanoes and other natural terrains using InSAR persistent scatterers. *Geophysical Research Letters*, **31**, L23611. doi:10.1029/2004GL021737.

Lanari, R., Casu, F., Manzo, M., Zeni, G., Berardino, P., Manunta, M. and Pepe, A., 2007, An overview of the Small BAseline Subset algorithm: a DInSAR technique for surface deformation analysis. *Pure and Applied Geophysics*, **164**, pp. 637–661.

Lanari, R., Mora, O., Manunta, M., Mallorquì, J.J., Berardino, P. and Sansosti, E., 2004, A small baseline approach for investigating deformation on full resolution differential SAR interferograms. *IEEE Transactions on Geoscience and Remote Sensing*, **42**, pp. 1377–1386.

Manzo, M., Fialko, Y., Casu, F., Pepe, A. and Lanari, R., 2012, A quantitative assessment of DInSAR measurements of interseismic deformation: the Southern San Andreas Fault case study. *Pure and Applied Geophysics (PAGEOPH)*, **169**, pp. 1463–1482.

Massonnet, D. and Feigl, K.L., 1998, Radar interferometry and its application to changes in the Earth's surface. *Reviews of Geophysics*, **36**, pp. 441–500.

Mora, O., Mallorquí, J.J. and Broquetas, A., 2003, Linear and nonlinear terrain deformation maps from a reduced set of interferometric SAR images. *IEEE Transactions on Geoscience and Remote Sensing*, **41**, pp. 2243–2253.

Pepe, A. and Lanari, R., 2006, On the extension of the minimum cost flow algorithm for phase unwrapping of multitemporal differential SAR interferograms. *IEEE Transactions on Geoscience and Remote Sensing*, **44**, pp. 374–2383.

Reilinger, R.E., Ergintav, S., Bürgmann, R., McClusky, S., Lenk, O., Barka, A., Gurkan, O., Hearn, L., Feigl, K.L., Cakmak, R., Aktug, B., Ozener, H. and Töksoz, M.N., 2000, Coseismic and postseismic fault slip for the 17 August 1999, M = 7.5, Izmit, Turkey earthquake. *Science*, **289**, pp. 1519–1524.

Shanker, A.P. and Zebker, H., 2010, Edgelist phase unwrapping algorithm for time series InSAR analysis. *Journal of the Optical Society of America A*, **27**, pp. 605–612.

Xu, W. and Cumming, I., 1999, A region-growing algorithm for InSAR phase unwrapping. *IEEE Transactions on Geoscience and Remote Sensing*, **37**, pp. 124–134.

Zebker, H.A. and Villasenor, J., 1992, Decorrelation in interferometric radar echoes. *IEEE Transactions on Geoscience and Remote Sensing*, **30**, pp. 950–959.